

Synthetic genotype networks

Javier Santos-Moreno^{1*}, Eve Tasiudi^{2*}, Hadiastri Kusumawardhani¹, Joerg Stelling^{2#}, Yolanda Schaerli^{1#}

1) Department of Fundamental Microbiology, University of Lausanne, Biophore Building, 1015 Lausanne, Switzerland

2) Department of Biosystems Science and Engineering, ETH Zurich and SIB Swiss Institute of Bioinformatics, Basel, Switzerland

* These authors contributed equally.

Corresponding authors: joerg.stelling@bsse.ethz.ch and yolanda.schaerli@unil.ch

Abstract

Genotype networks are sets of genotypes connected by small mutational changes that share the same phenotype. They facilitate evolutionary innovation by enabling the exploration of different neighborhoods in genotype space. Genotype networks, first suggested by theoretical models, have been empirically confirmed for proteins and RNAs. Comparative studies also support their existence for gene regulatory networks (GRNs), but direct experimental evidence is lacking. Here, we report the construction of three interconnected genotype networks of synthetic GRNs producing three distinct gene expression phenotypes in *Escherichia coli*. These genotype networks, composed of over twenty different synthetic GRNs, provide robustness in face of mutations while enabling transitions to innovative phenotypes. Through realistic mathematical modeling, we quantify robustness and evolvability for the complete genotype-phenotype map and link these features mechanistically to GRN motifs. Our work thereby exemplifies how GRN evolution along genotype networks might be driving evolutionary innovation.

Introduction

A *genotype network* (also called neutral network) (Ahnert, 2017; Lipman et al., 1991; Maynard Smith, 1970; Schuster et al., 1994; Wagner, 2005; Wagner, 2012) is a connected set of genotypes that produce the same phenotype. Within a genotype network, genotypes are directly connected to each other if they differ by a small mutational change. Genotype networks are thought to be a common organizational property of genotype spaces of biological systems at different levels. Ample empirical evidence for their existence supports this notion for RNAs (Bendixsen et al., 2019; Hayden et al., 2011; Schultes and Bartel, 2000), proteins (Baier et al., 2019; Bershtain et al., 2008; Bloom et al., 2007; Podgornaia and Laub, 2015; Zheng et al., 2019) and binding sites of regulatory proteins (Aguilar-Rodríguez et al., 2018; Anderson et al., 2015; Payne et al., 2018; Payne and Wagner, 2014).

In contrast, genotype networks of gene regulatory networks (GRNs) have remained more recalcitrant to investigations. This is an important limitation because GRNs underlie fundamental behavioural and developmental processes (Alon, 2006; Ptashne and Gann, 2002), and because understanding the relation between a GRN and its biological function (phenotype) is a central area of investigation in modern biology (Karlebach and Shamir, 2008). Current empirical evidence for the existence and features of genotype networks of GRNs is indirect. It mainly comes from comparative studies showing that rewiring of GRNs during the course of evolution does not necessarily alter the resulting gene expression pattern (Ewe et al., 2020; Haag, 2014; Hinman and Davidson, 2007; Kiontke et al., 2007; Wotton et al., 2015). Indeed, extensive rewiring seems to be very common (Dalal and Johnson, 2017; Johnson, 2017; Nocedal et al., 2017). Complementary theoretical studies revealed that a large number of different GRNs can produce the same phenotype and that many of those GRNs are interconnected by small mutational changes (Aguirre et al., 2018; Ciliberti et al., 2007a; Ciliberti et al., 2007b; Cotterell and Sharpe, 2010). However, these theoretical studies used abstracted models of GRNs not supported by experimental data.

Potential genotype networks for GRNs have three important implications. First, a genotype network of many GRNs can be traversed by making one mutational change at a time without losing the phenotype. Thus, a GRN is robust to those mutations that keep it on the same genotype network (Payne and Wagner, 2015). Second, a genotype network implies that the genotype can evolve while the phenotype is preserved. This is known as phenogenetic drift or system drift (True and Haag, 2001; Weiss and Fullerton, 2000), especially when referring to developmental GRNs. Thereby, genotype networks crucially contribute to evolutionary innovation (Payne and Wagner, 2019; Wagner, 2005): different genotypes at different positions within the genotype network provide access to genotypes that are part of adjacent genotype networks featuring distinct phenotypes. Consequently, evolving on a genotype network facilitates the exploration of different mutational neighborhoods in genotype space, which may harbor different phenotypes (Jimenez et al., 2015; Schaefer et al., 2018). Third, in some cases, the same specific mutation can have different

effects depending on the genotype where it occurs: some GRNs, when mutated, retain their phenotype and thus are part of the same genotype networks; the same mutation introduced into other GRNs can lead to mutant GRNs with a distinct phenotype. This common phenomenon, in which the effect of a mutation depends on the genetic background, is known as epistasis (Domingo et al., 2019).

Unfortunately, we still have very few experimentally accessible systems that allow us to understand comprehensively how GRNs map to their phenotypes, how they organize into genotype networks, and how these provide robustness to mutations and facilitate access to novel phenotypes (Crombach et al., 2016; Martchenko et al., 2007; Sorrells et al., 2015; Tsong et al., 2006). To address this issue, here we turned to synthetic biology, which allows us to build GRNs by assembling well-characterized parts that differ by small mutational changes. It also enables us to study GRNs without the common challenges and confounding factors associated with studying GRNs *in situ*, like unknown influence of the genetic background, high complexity and interconnectivity of the networks, and pleiotropy of their genes (Baier and Schaerli, 2021; Bayer, 2010; Crocker and Ilsley, 2017; Schaerli et al., 2018). Specifically, we decided to build a large set of synthetic GRNs based on CRISPR interference (CRISPRi) (Santos-Moreno et al., 2020) using *Escherichia coli* (*E. coli*) cells as host. Our GRNs differ from each other by small mutational changes, thus potentially creating genotype networks. As a starting GRN, we chose a type 2 incoherent feed-forward loop (IFFL-2) (Santos-Moreno and Schaerli, 2019b), which is commonly found in natural systems, including in developmental processes of multicellular organisms such as *Drosophila* blastoderm patterning (Jaeger, 2011). In response to a chemical concentration gradient, its phenotype can be a “stripe” of gene expression (low–high–low), analogous to the formation of spatiotemporal gene expression patterns guided by morphogen gradients during development (Rogers and Schier, 2011; Sagner and Briscoe, 2017). Overall, we report the construction and experimental exploration of three synthetic genotype networks, each composed of a group of interconnected GRNs and displaying a distinct phenotype, as well as the generalization to the complete genotype-phenotype map using mathematical modeling.

Results

A genotype network of GREEN-stripe GRNs

We previously described a synthetic GRN with an IFFL-2 topology that governs the spatial patterning of a population of *E. coli* cells (Santos-Moreno et al., 2020). Our synthetic IFFL-2 responds to a gradient of arabinose (Ara) and produces a stripe of green fluorescence (**Fig. 1A**). It consists of three nodes connected by repression interactions so that the input node (orange) represses both the intermediate (blue) and the third (green) nodes, and the intermediate represses the third node as well (**Fig. 1A**). The input node (orange) expression rises with increasing Ara

levels. The repression logic produces a concomitant decrease of expression in the intermediate node (blue); consequently, expression of the third node (green) is highest where combined levels of the other nodes is lowest, resulting in a stripe (peak) of gene expression at intermediate Ara concentration (**Fig. 1A**). In our GRN, this behavior can be easily monitored by fluorescence reporters present in each node: mKO2 (orange), mKate2 (red, here represented in blue for clarity) and sfGFP (green). More specifically, repression is based on CRISPR interference (CRISPRi). A repressing node produces single guide RNAs (sgRNAs) that recognize specific target binding site (bs) sequences downstream of the promoters in the node to be repressed. CRISPRi-based repression constitutes a versatile framework for synthetic GRN construction due to high programmability and orthogonality and low incremental burden (Santos-Moreno and Schaeferli, 2020; Santos-Moreno et al., 2020), and we can easily construct new GRN variants with a previously described modular cloning strategy (Santos-Moreno and Schaeferli, 2019a).

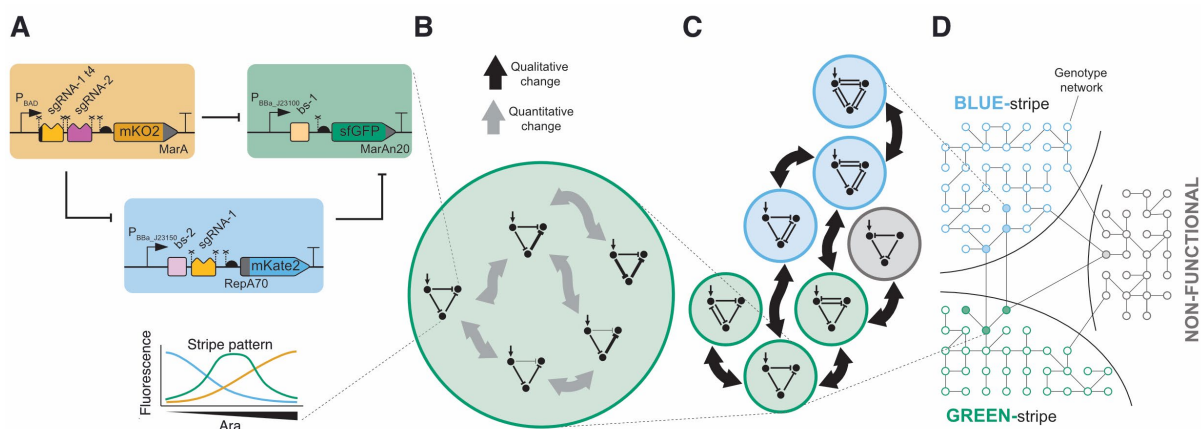


Fig. 1. Overview of three interlinked genotype networks of synthetic GRNs built in this study that produce distinct phenotypes for stripe formation: BLUE-stripe, GREEN-stripe, and non-functional. The different levels of organization are depicted. **A.** Details of the molecular implementation of one GRN (GRN 1.1 from **Fig. 2**), with the resulting GREEN-stripe phenotype schematically depicted below. Key to symbols: Bent arrows: promoters; squares: sgRNA binding sites; jagged rectangles: sgRNAs; crosses: *csy4* recognition sites; semicircles: ribosome binding sites (RBSs); pointed rectangles: reporter genes; and T-s: transcriptional terminators. MarA, MarAn20 and RepA70 denote orthogonal degradation tags. **B.** For a GRN topology, there might exist multiple interlinked GRN variants with different parameters that preserve the same phenotype (here shown as connected if they differ by a single parameter change, either qualitative or quantitative). **C.** We built several topologies (colored according to the phenotype) that connect within and between genotype networks. **D.** The topologies in (C) are part of larger genotype networks that share the same phenotype. Each node in the genotype networks represents one GRN topology with an edge between two nodes if topologies can be interconverted with a single mutational change.

To construct a synthetic genotype network, we applied two types of changes to GRNs (**Fig. 1B-C**): qualitative ones, where interactions are gained or lost and thus the topology (i.e. the wiring) of the network changes, and quantitative ones, where the strengths of the regulatory interactions (i.e. the parameters) change (Crombach et al., 2016). Here, we modified topologies by adding or removing repression interactions. As for parameters, we modulated them in two ways: first, through the choice of three promoters (low, medium, high) that govern transcription of the nodes; and second, by employing four sgRNAs with different strengths. We also used two truncated versions ('t4', truncation of the four 5' nucleotides) of the sgRNAs, which provides another way to tune repression strength (Santos-Moreno et al., 2020). We consider each of these modifications as a single mutation and quantify relations between quantitative and qualitative changes using mathematical models.

Starting from the original GRN (**Fig. 2**, design 1.1), which produces a GREEN-stripe pattern in a gradient of Ara, we first introduced quantitative changes without modifying the GRN topology. Replacing sgRNA-1t4 with its full-length version to yield GRN 1.2 only slightly decreased the height of the stripe (**Fig. 2**, design 1.2). A significant increase in the strength of the blue node's promoter in GRNs 1.3 and 1.4 resulted in stripes being asymmetric and shifted towards higher Ara concentrations (**Fig. 2**, designs 1.3 and 1.4). Thus, the quantitative modifications preserved the GREEN-stripe, but they affected the shape of the stripe.

Previous theoretical work suggested that other GRN topologies populate the same genotype network as our IFFL-2 (Arboleda-Rivera et al., 2022; Cotterell and Sharpe, 2010; Schaerli et al., 2014). To explore those, we next increased GRN complexity by adding one extra repression. Addition of sgRNA-4t4 or of the full-length version sgRNA-4 from the green node to the orange node indeed preserved the GREEN-stripe (**Fig. 2**, GRNs 2b.1 and 2b.2). Alternatively, we also added a new repression from the blue to the orange node (instead of green to orange) to produce yet a different topology, GRN 2a.1, also displaying a GREEN-stripe phenotype (**Fig. 2**). Overall, these GRNs demonstrate an uninterrupted genotype network: single (qualitative or quantitative) mutations connect the GRNs, such that distant GRNs are connected by intermediates that preserve the same common phenotype.

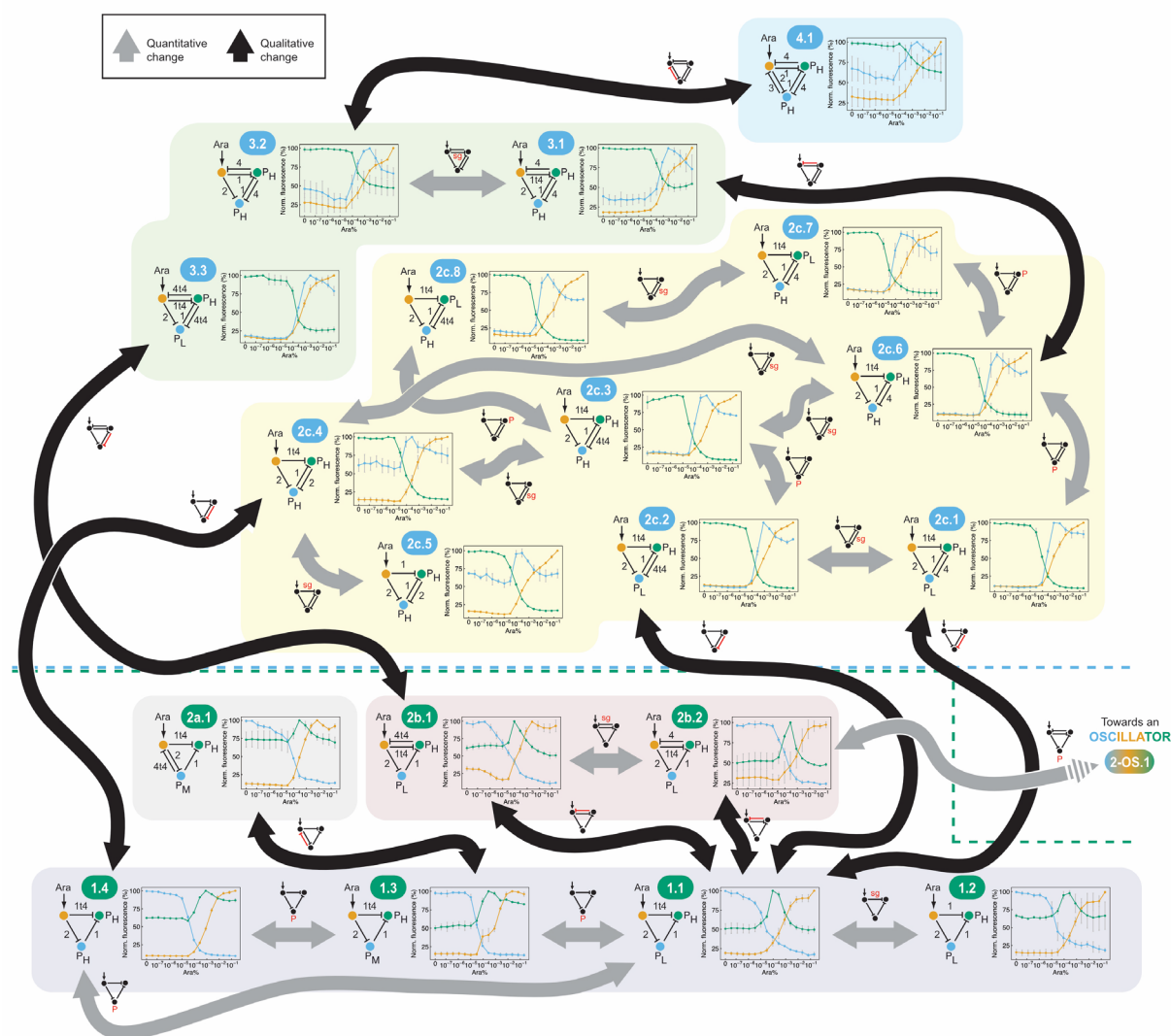


Fig. 2. A synthetic genotype network of GREEN-stripe (bottom) and BLUE-stripe (top) GRNs. Starting from a CRISPRi-based GREEN-stripe incoherent feed-forward loop (IFFL-2, design 1.1), we introduced quantitative (gray) or qualitative (black) changes to produce a genotype network of synthetic GREEN-stripe GRNs. Single changes enabled the transition from GREEN-stripe GRNs to BLUE-stripe GRNs. We then explored this BLUE genotype network through parameter (gray) or topology (black) changes, up to the GRN with the maximum number of repressions for a 3-node GRN without self-repression, GRN 4.1. Dashed lines represent the boundaries of the GREEN-stripe and BLUE-stripe genotype networks. Each design is denoted with a unique code displayed in an ellipse (color-coded according to the phenotype), with the details of the design provided in the diagrams below. The GRN code denotes both the complexity (i.e. number of interactions) and the topology, as well as the specific implementation. A higher starting number of the GRN (e.g. 2 vs. 1) reflects an increased complexity, while different topologies sharing the same complexity are denoted with different letters (e.g. 2a vs. 2b). Lastly, the final number (e.g. 2b.1 vs. 2b.2) distinguishes specific implementations within the same topology. Numbers by the repressions indicate the identity of the sgRNAs, while P_H , P_M and P_L represent constitutive promoters.

(BBa_J23100, BBa_J23102 and BBa_J23150, respectively). Small GRNs by the arrows display the changes (in red) between the connected GRNs: topology changes (T) or changes in the promoter strength (P) or in the identity of the sgRNAs (sg). The phenotype of each GRN was characterized in a microplate reader by determining the fluorescence of the three protein reporters (mKO2 (orange), sfGFP (green) and mKate2 (red, here depicted in blue for clarity)) as a function of arabinose (Ara) concentration. Data show the mean three biological replicates, with error bars depicting s.d. of normalized replicates (n=3). GRNs sharing a common topology are grouped with a colored background. The dashed arrow indicates transition towards another synthetic genotype network (that of oscillators, see **Fig. 7**).

A genotype network of BLUE-stripe GRNs

To explore a different genotype network, we noted that adding a repression from the green node to the blue node to the original GRN (1.1) makes the topology completely symmetrical. In this topology, either the green or the blue node can form a stripe, depending on the parameters. Adding the repression to two different GREEN-stripe GRNs (**Fig. 2**, GRNs 1.1, 1.4) inverted the roles of the two nodes, producing a BLUE-stripe, with the green node now decreasing with increasing Ara concentration (**Fig. 2**, GRNs 2c.1, 2c.2, 2c.4). A series of control GRNs confirmed that the GREEN- to BLUE-stripe transition is a consequence of the action of the sgRNA added, and not some spurious context-dependent effect (**Fig. S1**). Thus, a single mutation in some of the GRNs of the GREEN-stripe genotype network suffices to achieve a new phenotype, highlighting the potential of genotype networks for evolutionary innovation.

As already observed for the GREEN-stripe GRNs, quantitative changes in the promoter and/or the sgRNA strengths yielded new BLUE-stripe GRNs in an interlinked network (**Fig. 2**, GRNs 2c.1 to 2c.8). Many of these GRNs produce skewed BLUE-stripes, but one GRN shows a remarkable symmetry, both in the design and in the phenotype (**Fig. 2**, GRN 2c.5).

To assess robustness of the BLUE-stripe genotype network to topological changes, we further increased complexity to five repression interactions. Adding a new sgRNA from green to orange node resulted in GRNs 3.1 to 3.3, all of which produce a BLUE-stripe (shifted to higher Ara concentrations; **Fig. 2**). Interestingly, this 5-repression BLUE-stripe producing topology can be accessed from a 4-repression topology with either a BLUE-stripe (2c.6 to 3.1 transition) or a GREEN-stripe (2b.1 to 3.3 transition). The 5-repression GRN 3.2 in turn served as the basis for building a GRN with six repressions between the three nodes – the theoretical maximum number of repressions for a 3-node GRN without self-repression (**Fig. 2**, GRN 4.1). This design produces a stripe similar to the other ones in its genotype network. In summary, we explored a genotype network of synthetic BLUE-stripe GRNs; these GRNs are connected not only among themselves, but also to the genotype network of the GREEN-stripe GRNs (**Fig. 2**).

Ensemble mathematical modeling predicts genotype-phenotype relations

In our synthetic implementations, we explored a large set of functional GRNs (19 3-node GRNs) thanks to the versatility of CRISPRi. Yet, compared to the total number of 1'873'152 possible implementations (42 topologies with 3 to 6 edges, each with 6 possible sgRNAs and 3 promoter efficiencies), this set was too small to conclude quantitatively on robustness and evolvability of genotype networks for GRNs. In addition, some experimental findings required mechanistic interpretations, for example, why we always observed a BLUE-stripe whenever a repression from the green node to the blue node was present. We therefore developed mechanistic mathematical models to explore the full genotype space *in silico* on the one hand, and to analyze mechanisms and guide experimental design on the other hand.

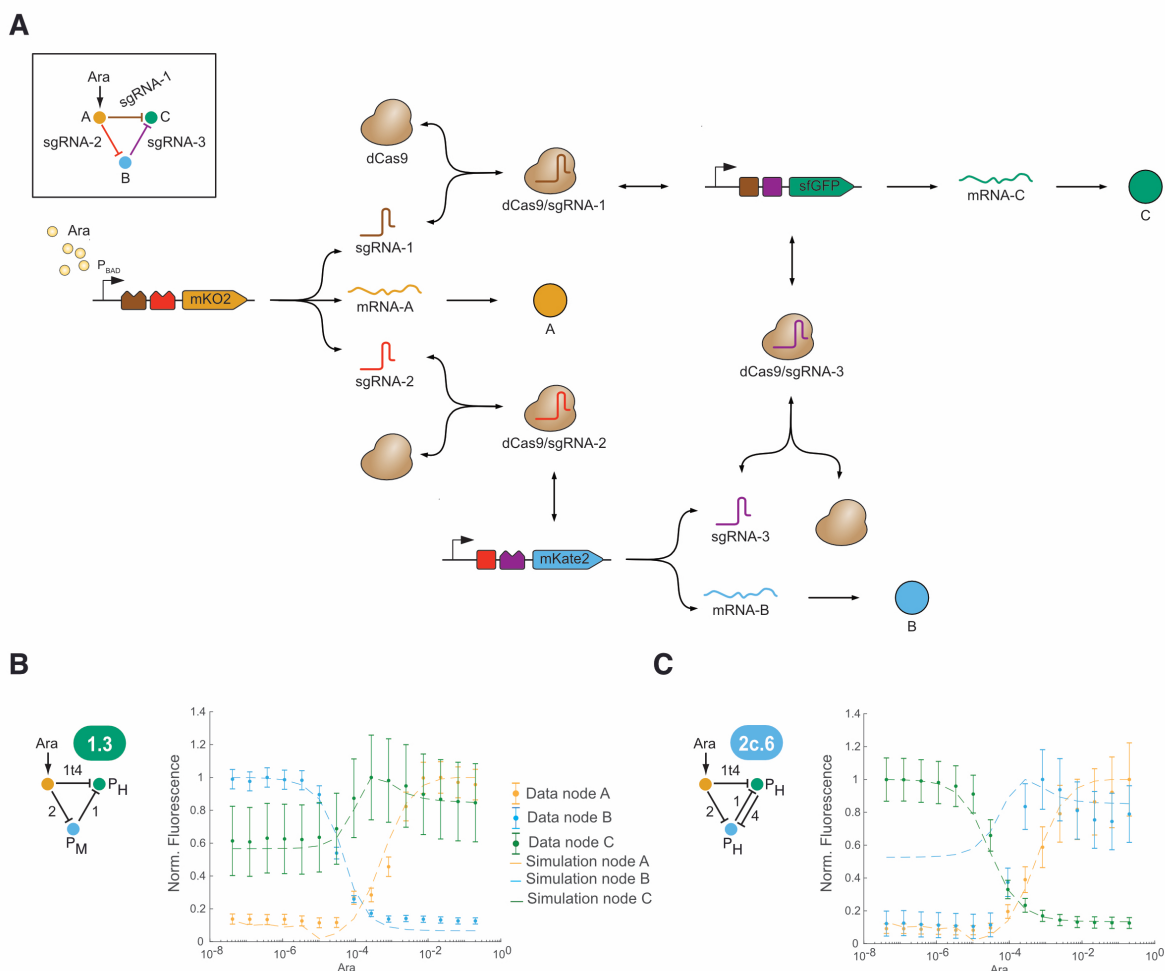


Fig. 3. Model overview and predictions. A. Model components and processes for the example of an IFFL-type 2 using generic sgRNAs 1-3 (inset). Arabinose induces expression of sgRNA-1 (brown jagged rectangle), sgRNA-2 (red) and A (orange). sgRNA-1 and sgRNA-2 form complexes with dCas (brown), and A undergoes translation (mRNA-A) and maturation (A). sgRNA-3 (purple), B (blue) and C (green) are constitutively expressed (bent arrows). sgRNA-3 forms a complex with

dCas, and B and C are translated (mRNA-B, mRNA-C) and mature (B,C). sgRNA/dCas complexes can bind to their target sites (brown, red, and purple squares) and inhibit gene expression. RNAs are subjected to active degradation, proteins (A, B, C) to active degradation and dilution, and complexes to dilution. **B, C.** Independent model predictions (dashed lines) compared to experimental data (symbols, as in **Fig. 2**) for two example GRNs (see also **Fig. S2**). Models were adapted to account for the sgRNAs in the implemented GRNs. Error bars show s.d. based on error propagation, n=3 independent experiments.

The models represent detailed interactions between Ara-controlled gene expression, sgRNA and fluorescent protein expression, dCas9-sgRNA interactions, CRISPRi-mediated control of gene expression, and component degradation or dilution, as illustrated in **Fig. 3A** for an IFFL-type 2 GRN. To capture the experiments conducted in microplate readers realistically, we included simplified model components for microbial growth and fluorescent protein maturation into the dynamic (ordinary differential equation-based) models; the overall model structure allowed to specify all possible topologies and parametrizations (see **Methods** for details). For model calibration, we used experimental data for two-node GRNs with different sgRNAs (Santos-Moreno et al., 2020), and for a selection of three-node GRNs (**Fig. S2**). Importantly, we constrained parameters to map 1:1 to biological components, such that a specific sgRNA or promoter had the same value for, e.g., affinity constants, throughout all models (see **Methods**). In principle, this enables predictions for the entire genotype space of GRNs implementable with the synthetic parts used.

The models faithfully predicted the experimentally observed behaviors of GRNs that differed in topologies or parts from those used in model calibration (i.e., the independent validation set), as shown in **Fig. 3B,C** and **Fig. S2**. In addition, the inferred sgRNA affinities were qualitatively consistent with measured repression strengths (**Data S1**). Overall, we conclude that the mathematical models are sufficiently realistic for comprehensive *in silico* analyses.

Models enable a comprehensive analysis of robustness and evolvability

To assess the global genotype-phenotype (GP) map, we predicted the behavior of all 1'873'152 possible GRNs and established three phenotypes for stripe formation: BLUE-stripe, GREEN-stripe, and non-functional (NF; see **Methods** for definitions). For the genotypes, each parametrized model (i.e., representing a GRN) is a genotype and a single mutation amounts to a change in one parameter value. Note that such a parametric change may also alter the topology, for example, by effectively eliminating a repressive interaction. The summary in **Fig. 4A** shows that functional GRNs (GREEN- and BLUE-stripe GRNs) are relatively rare (77% NF, 11% BLUE-stripe and 11% GREEN-stripe), both in terms of topologies and of GRNs within a topology, consistent

with previous results for RNAs and proteins (Ahnert, 2017). In more detail, as suggested by our experimental data, mutual inhibition of green and blue nodes is required to enable a topology that shows both BLUE- and GREEN-stripe phenotypes.

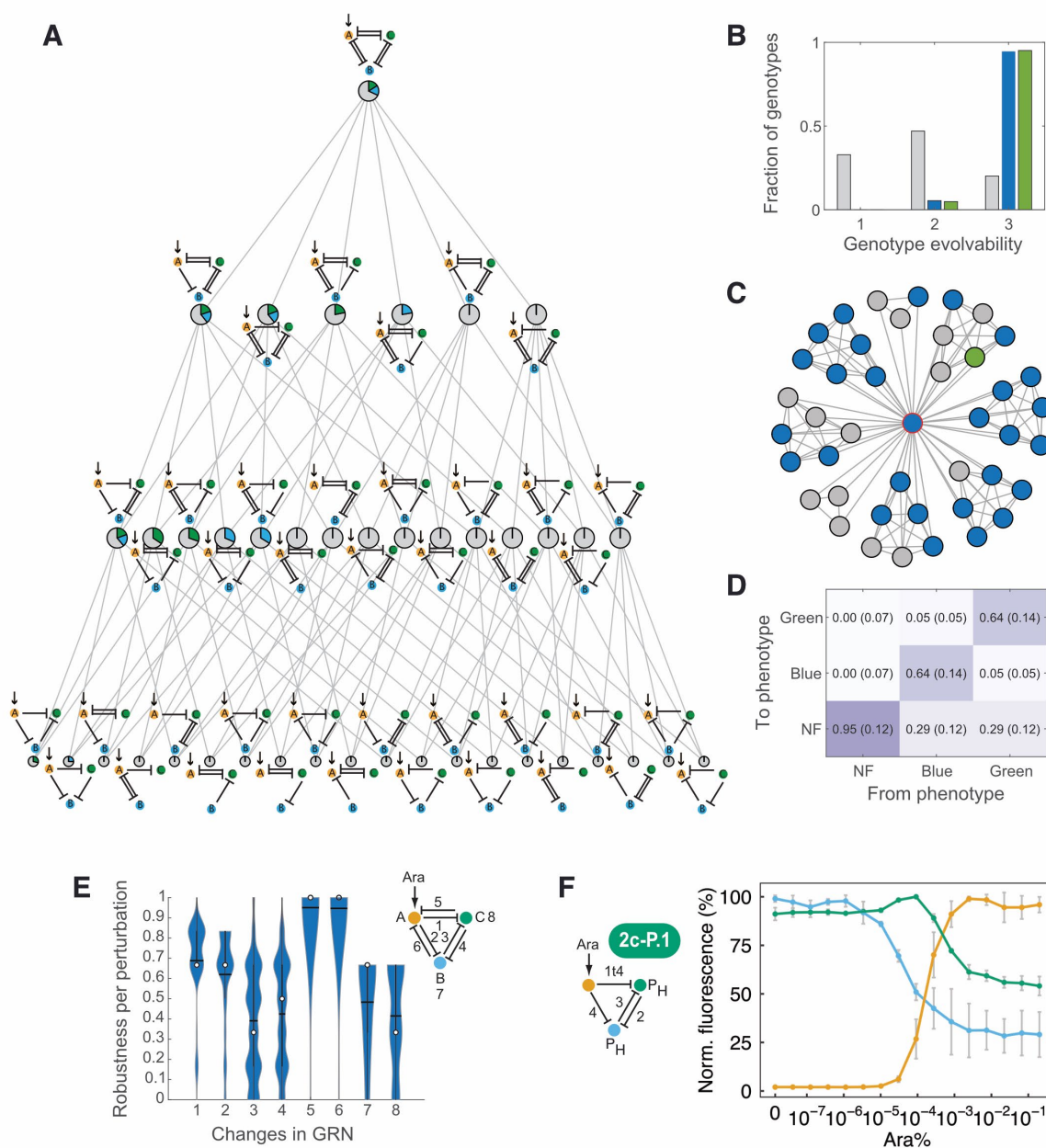


Fig. 4. Model-predicted robustness and evolvability. **A.** Network topologies (schemes as in **Fig. 1**) and their neighbor relations (grey lines indicating that GRNs in two topologies are reachable by a single mutation). Pie charts indicate fractions of GRNs (genotypes) with BLUE-stripe (blue), GREEN-stripe (green) and non-functional (NF; grey) phenotype per topology. **B.** Distributions of evolvability (number of phenotypes in the 1-neighborhood of a genotype) for genotypes with BLUE, GREEN, and NF phenotype (colors as in **(A)**). **C.** Example subgraph for the red-circled node with evolvability 3 and its direct neighbors (27 BLUE-, 1 GREEN-stripe and 14 NF, colors as in **(A)**). **D.** Transition frequencies (median, interquartile range in brackets) between indicated phenotypes

resulting from transitions between neighboring genotypes. **E.** Robustness (fraction of neighboring genotypes with the same phenotype as a given genotype) classified by type of perturbations (indicated by numbers in GRN diagram), namely changes of sgRNA type (1-6) and promoter strengths (7-8) for the respective interactions and nodes for GRNs with BLUE-stripe phenotype. **F.** Experimental test of a model prediction to convert a BLUE-stripe GRN to a GREEN-stripe GRN with the same topology; symbols as in **Fig. 2**.

Surprisingly, we found that the BLUE-stripe, GREEN-stripe, and NF genotype networks were each composed of a single connected network (a strongly connected component in graph terms). Hence, it is possible for very different GRNs to establish the same phenotype and to reach any of these GRNs in single mutations without changing the phenotype. To analyze the GP map in more detail, we first determined genotype evolvability, defined as the number of phenotypes accessible from a GRN in a single mutation change (i.e., in the 1-neighborhood of a GRN in the genotype network) (Wagner, 2008). Most functional GRNs were adjacent to at least one GRN of all the other phenotypes, in contrast to the NF GRNs (**Fig. 4B**), indicating high evolvability of functional GRNs specifically. However, this adjacency does not imply that it is likely that a mutation will yield a new (specific) phenotype, for example, when this phenotype is rare in the neighborhood, as illustrated in **Fig. 4C**. We therefore analyzed possible transitions between phenotypes (**Fig. 4D**). Entries on the diagonal show that NF GRNs are highly robust to mutations, and functional ones moderately robust. Transitions to a NF phenotype dominate for all GRNs, but switching between a BLUE- and GREEN-stripe has a substantial probability. To make these results more interpretable, we used random walks on the genotype network to determine the mutational path lengths for altering phenotypes (see **Methods**). Median path lengths were 2 for functional GRNs and 18 for NF GRNs (**Fig. S3**), representing a high evolutionary barrier to establish function, but high evolvability of function. Importantly, when we repeated the analysis with additional artificial inhibition and promoter strengths (see **Methods**) as a control, results were very similar (**Fig. S4**).

To relate this analysis to our synthetic biology approach in more detail, we determined robustness to changes in GRN parts and interactions. Over all genotypes, phenotypes were most sensitive to alterations of promoter strengths for the blue and green nodes, and (in a bimodal manner) of sgRNA-mediated interactions between these two nodes (**Fig. 4E** and **Fig. S3**). To test these predictions, we asked how we could convert the phenotype of topologies that theoretically afford both functional phenotypes, but for which we experimentally observed only BLUE-stripes. Specifically, we used the models to predict modifications of GRNs in our experimentally implemented BLUE-stripe genotype network that yield a GREEN-stripe. The requirements to swap between the functional phenotypes mirrored the parameter sensitivities (**Fig. 4E**), namely promoter and inhibition strengths between the blue and green node. Similar to (Munteanu et al., 2014), we predicted that a stronger inhibition (higher sgRNA affinity) on the green node with the correct promoter efficiencies for both green and blue node was enough to alter the phenotypes. In

experiments, GRN 2c-P.1 indeed showed a phenotype switched to GREEN-stripe, as illustrated in **Fig. 4F**. Thus, our models provide global as well as detailed, experimentally actionable, analyses of GRN robustness and evolvability.

Combining IFFL and mutual inhibition enhances evolvability

To understand mechanisms in biological networks, a powerful approach is to focus on the topology, and specifically on network motifs, small sub-networks that are critical for function and reveal design principles (Alon, 2007). For example, they helped investigate robustness and (to a certain extent) evolvability of the gap gene patterning system of insects (Verd et al., 2019). However, a systematic analysis of GP maps in terms of topologies and motifs is non-trivial because, for example, here the number of GRNs per topology varies between 3'456 and 746'496.

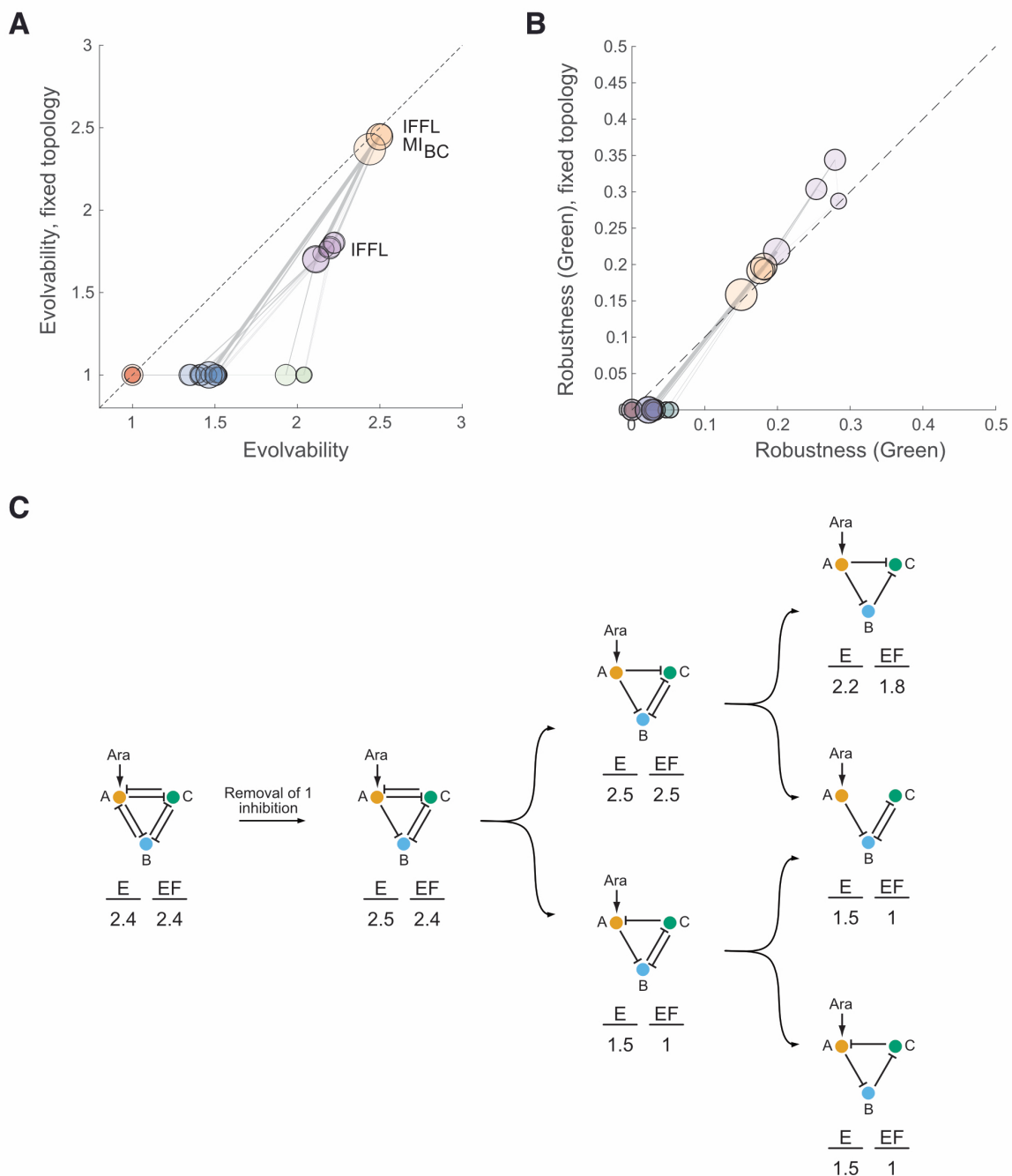


Fig. 5. Mechanistic basis of robustness and evolvability. **A.** Average predicted phenotypic evolvability per topology (circles) over all neighboring genotypes (x-axis) vs only genotypes with the same, fixed topology (y-axis). Topologies were clustered (indicated by colors; k-means clustering with k=5). Circle sizes reflect numbers of repressive interactions in a topology and grey lines link adjacent topologies as in **Fig. 4A**. The dashed diagonal indicates equal evolvability with and without fixed topology. MI_{BC}: mutual inhibition of nodes B (blue) and C (green). **B.** Quantification of robustness for the GREEN-stripe phenotype; results shown as in **A**, with the same coloring of clusters. **C.** Example for the effect of transitions between topologies (arrows: removal

of one inhibitory interaction) on average evolvability (E) and evolvability with fixed topology (E_F) measured as in **A**.

We propose to address this challenge by computing genotypic robustness and evolvability in two ways: (i) for the entire 1-neighborhood of each GRN and (ii) for only those neighbors of a GRN that have the same topology. The results for evolvability in **Fig. 5A** show a clear differentiation of topologies into five clusters (see also **Supplementary Table 2**). Topologies that are always non-functional (evolvability of one with fixed topology) can only become functional when evolving (directly or indirectly) to topologies containing an IFFL. Evolvability increases further by incorporating a mutual inhibition (MI) of blue and green nodes, complementing our earlier observations. Importantly, these network motifs, and not GRN complexity (i.e. number of interactions) determine evolvability.

Regarding robustness (**Fig. 5B** for the GREEN-stripe phenotype, and **Fig. S2**), functional GRNs – those with an IFFL – perform substantially better than the other GRNs. In contrast to evolvability, including the MI motif decreases robustness of a given functional phenotype, again not correlated with GRN complexity. This is consistent with a previously observed trade-off between genotypic evolvability and robustness (Payne et al., 2014), but apparently contradicts the finding that complexity aids robustness (Catalán et al., 2018), both derived from abstractly modeled GRNs. We argue that experimentally validated GRN models and their analysis via network motifs provide a more realistic and mechanistically interpretable view, as illustrated in **Fig. 5C**.

Epistatic interactions within the BLUE-stripe genotype network

A third aspect important for evolution is the existence and prevalence of epistatic interactions; small sample sizes make the latter difficult to estimate *in vivo*, but a recent analysis in yeast showed a prevalence of ~3% (Nguyen Ba et al., 2022). To relate to genotype networks, we focused on one type of epistasis, namely where two sequential changes ('A' and 'B') allow genotype network exploration without a phenotype loss, while the same changes in the reverse order (first 'B' then 'A') goes along with a loss of the phenotype after the first change (**Fig. 6A**). Our models predict median prevalences of ~4.5% for functional GRNs, and a lower one for non-functional GRNs (~2.5%) (**Fig. 6B**). This is qualitatively consistent with prior experimental studies; it highlights again the need to differentiate between functional and non-functional phenotypes.

In our synthetic GRNs, we also discovered that the order of the changes actually matters. We found an instance of epistasis in the transition from topology 2c to topology 3. Starting from GRN 2c.6, the addition of sgRNA-4 from green to orange node yielded the functional GRN 3.1, which could then be modified by replacing sgRNA-1t4 with its stronger repressing full-length version to produce GRN 3.2, also functional (**Fig. 6C**). However, the same changes in the reverse

order required traversing through a non-functional intermediate, GRN 2c-NF.1, implying that strengthening the repression from the orange to the green node was only tolerated if an opposing interaction was present. These findings underline the usefulness of combining synthetic GRNs and modeling to analyze genotype networks comprehensively.

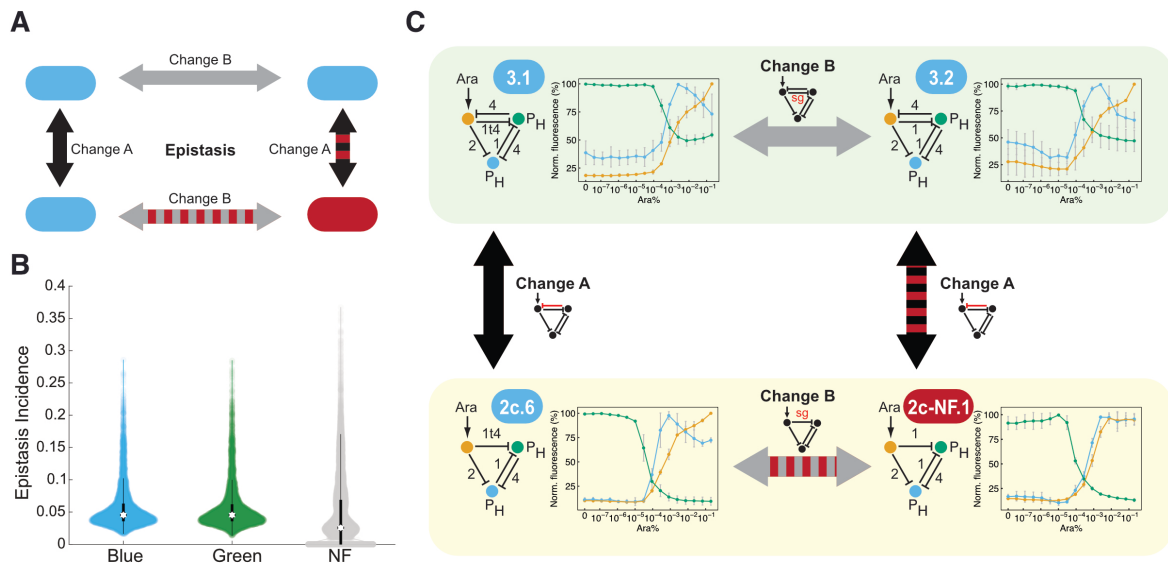


Fig. 6. Epistatic interactions. **A.** Schematic illustration of epistasis. Two consecutive changes 'A' and 'B' allow for a smooth 'walk' within the BLUE-stripe genotype network. However, the same changes in the reverse order transition through a GRN that is in the non-functional genotype network. **B.** Model-based estimation of epistasis incidence by sampling 5% of pairs of GREEN and BLUE, and 2% of NF GRNs within their corresponding genotype network. Circles: median; vertical lines: interquartile range. **C.** Experimental demonstration of epistasis. The transition from GRN 2c.6 to 3.2 within the BLUE-stripe genotype network requires two changes in a specific order, via intermediate 3.1. The reverse order of changes involves a non-functional intermediate, 2c-NF.1. Grey arrows: parameter changes; black arrows: topology changes; red shading: connections from / to non-functional GRNs.

A genotype network of oscillating GRNs

Finally, to evaluate if our findings on the existence of genotype networks translates to other definitions of phenotypes, we exploited prior theoretical work. It demonstrated that GRNs with topologies like GRN 2b.2 can produce temporal oscillations (Li et al., 2012; Panovska-Griffiths et al., 2013; Perez-Carrasco et al., 2018; Verd et al., 2019) – its topology actually contains that of the repressilator, a well-known molecular oscillator (Elowitz and Leibler, 2000). In addition, we

previously demonstrated that CRISPRi can be employed to build a repressilator – a circuit that we named the CRISPRlator (Santos-Moreno et al., 2020).

Starting from GRN 2b.2, a single parameter change (a stronger promoter in the blue node) sufficed to produce an oscillatory phenotype, as assessed through a continuous characterization of the gene expression dynamics in a microfluidic device (**Fig. 7**, GRN 2-OS.1). The removal of sgRNA-1t4 did not abolish oscillations and indeed rendered the topology closer to that of the classical repressilator; substituting the reporters with ones better suited for our microscopy settings also preserved the oscillatory dynamics (**Fig. 7**, 1-OS.1 and 1-OS.2). Finally, the replacement of P_{BAD} with a constitutive promoter (P_H) recreated the previously reported CRISPRlator displaying highly regular oscillations (**Fig. 7**, 1-OS.3). Hence, a genotype network composed of synthetic GRNs that enables exploration of the genotype space without a phenotype loss, and facilitates innovation by providing access to novel phenotypes in their neighborhoods exists also for dynamic phenotypes.

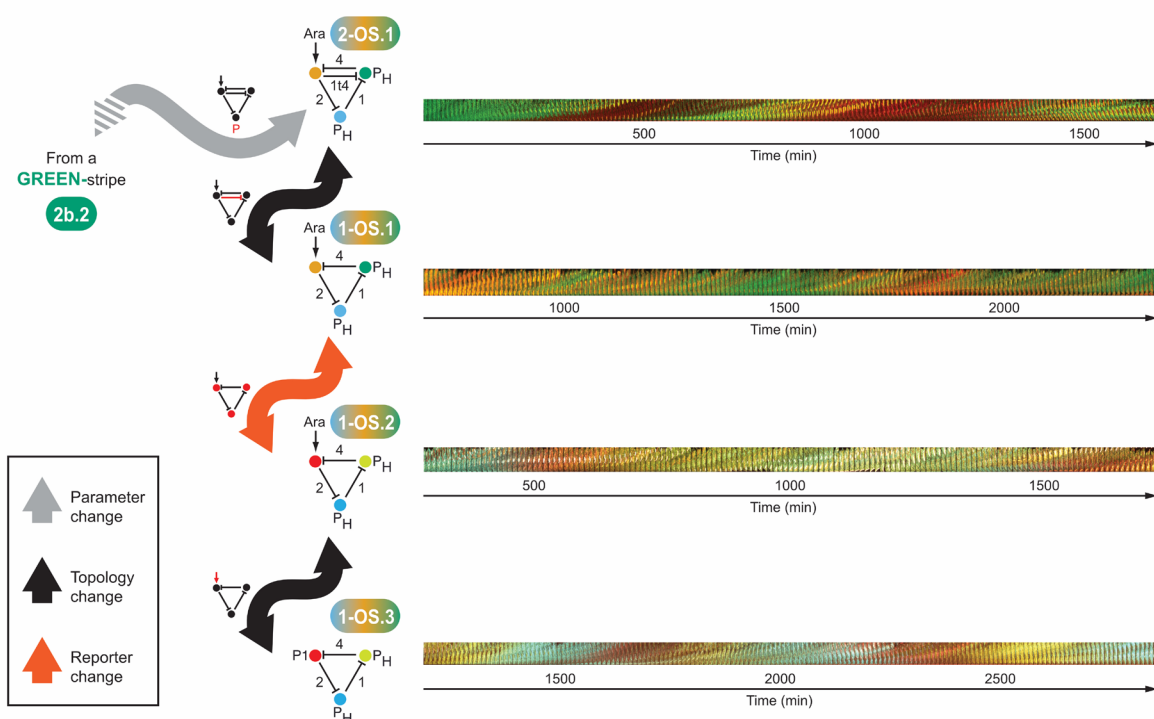


Fig. 7. A synthetic genotype network of oscillatory GRNs. Starting from the GREEN-stripe GRN 2b.2, a stronger promoter for the blue node leads to a GRN that displays oscillatory expression. Few changes suffice to transition to the CRISPRlator (Santos-Moreno et al., 2020), with all intermediates showing the oscillatory phenotype. Bacteria carrying the indicated GRNs were grown in continuous exponential phase in a microfluidic device and imaged every 10 min for up to two days. Oscillations are shown as kymographs: images of the microfluidic chamber (hosting ~100 cells) are displayed in order in a timeline montage. Due to an overlap of mKO2 and mKate2 in the same channel, red color for 2-OS.1 and 1-OS.1 (top) represents both mKO2 and mKate2,

while green corresponds to sfGFP. Different fluorescent reporters mCherry (red), mCitrine (yellow) and Cerulean (blue) allowed us to characterize the dynamics of all three nodes (1-OS.2 and 1-OS.3; bottom).

Discussion

Synthetic biology has recently been used to address fundamental questions in molecular evolution of regulatory networks (Chau et al., 2012; Igler et al., 2018; Isalan et al., 2008; Lagator et al., 2017; Schaeerli et al., 2018). Taking advantage of synthetic biology tools allowed us to assess several key features of GRN genotype networks experimentally and theoretically. We demonstrate that distinct synthetic GRNs can indeed be part of the same genotype network in which small mutational changes enable the smooth transition between any two GRNs without losing the target phenotype. On the other hand, genotypes very close in mutational distance can have distinct phenotypes, and genotypes in different positions of the genotype network can access different novel phenotypes. More specifically, our results conform to a ‘bowl of spaghetti’ metaphor known from the RNA world (Ahnert, 2017; Goldstein, 2008), but with subtle differences in the robustness and evolvability of GRN function. Both the connectedness of genotype networks and that they spread throughout the genotype space were proposed to be crucial for robustness and evolutionary innovation (Wagner, 2011). Our study provides experimental as well as theoretical evidence for it. Importantly, this is not restricted to stripe-forming GRNs. For example, our data suggests an evolutionary trajectory from a GREEN-stripe to an oscillatory GRN.

Prior theoretical work on GRNs highlighted that the definition of mutations is crucial for the analysis of robustness and evolvability, but it used abstract concepts such as signal-integration logic (Payne et al., 2014). Here, quantitative changes involve mutations in DNA sequences encoding both *cis*-regulatory elements (promoters) and *trans*-regulatory factors (sgRNAs). The three constitutive promoters used in this study differ in 2 - 4 nucleotides. Mutations in *trans* involve a 4 nt difference between full-length or truncated sgRNAs or changing the DNA-binding part of the sgRNA (20 nt). Such small differences in *cis*- or *trans*-regulatory regions have been found to play a role in the evolution of natural networks (Wray, 2007). Qualitative changes between our GRNs involve the gain or loss of a sgRNA and its corresponding binding site. Comparative studies show that rewiring within transcriptional networks is common in natural systems, often facilitated by duplication events and subsequent diversification (Voordeckers et al., 2015). Our transitions in genotype space include duplications of a regulatory element (e.g., from GRN 1.4 to 2c.4: a new sgRNA-2 in the green node binds to the existing bs-2 in the blue node), binding site duplications (e.g., from GRN 2c.6 to 3.1: the existing sgRNA-4 in the green node binds to a new bs-4 in the orange node), and combinations of both (e.g., from GRN 1.1 to 2b.2: a new sgRNA-4 in the green node binds to a new bs-4 in the orange). Hence, our synthetic GRNs and their mathematical

models – while not representing individual mutations at the DNA level – incorporate realistic single mutational changes in evolutionary trajectories.

Another critical aspect is the selection of phenotypes, and correspondingly the phenotypic space. Our GRNs displayed phenotypes – stripe formation in a gradient and oscillations – that are crucial for metazoan development of many organisms and body structures (Rogers and Schier, 2011; Sagner and Briscoe, 2017). We used coarse-graining (e.g., BLUE-stripe, GREEN-stripe, and NF) to characterize these phenotypes. It is a justified simplification and common practice when studying the evolution of GRNs (Cotterell and Sharpe, 2010; Cotterell and Sharpe, 2013; Friedlander et al., 2017; Schaefer et al., 2018). However, because the underlying experimental and simulation data is quantitative, our coarse-graining is already a step towards a more realistic scenario than Boolean logic behaviors (Alon, 2007; Payne and Wagner, 2013). Correspondingly, GRNs in one of our genotype networks may display quantitatively different behaviors. In a natural system, many of these differences could be buffered downstream (Floc'hlay et al., 2021), while others might lead to different organismal features. Coarse-graining to only three phenotypes for stripe-forming GRNs, however, implied that we could not study phenotypic robustness and evolvability. They are suggested to exhibit subtle, yet important differences to their genotypic counterparts (Payne and Wagner, 2019) and could be addressed in future studies.

We combined experiments and modeling to characterize the GP map of our synthetic GRNs realistically and comprehensively; neither of the two approaches alone could achieve this. It allowed us to link robustness and evolvability to small network motifs. Even when embedded in larger networks, motifs are necessary and sufficient for many network functions (Alon, 2007). For example, one of the best studied GRNs, the gap gene network in insects, comprises several genes that regulate each other by intricate repression motifs (among them IFFL-2) to produce stripes of gene expression that eventually establish anterior-posterior embryo segmentation (Wotton et al., 2015). Comparative analysis in different dipteran insects provides strong evidence for system drift and evolution on a genotype network (Crombach et al., 2016; Jaeger, 2018; Wotton et al., 2015). Interestingly, *Anopheles gambiae* and *Drosophila melanogaster* have inverted stripe expression patterns of the gap genes *giant* (gt) and *hunchback* (hb) (Goltsev et al., 2004; Wotton et al., 2015). Given the potential for simple mutational changes to switch between GREEN- and BLUE-stripe in IFFL-2-based synthetic GRNs, our work provides possible evolutionary paths for this role-switching in dipteran gap GRNs.

Similarly, the network topology of 2-OS.1 is known as AC-DC (Panovska-Griffiths et al., 2013; Perez-Carrasco et al., 2018). It is involved in patterning the vertebrate neural tube (Balaskas et al., 2012) and in the *Drosophila melanogaster* gap gene network (Verd et al., 2019). Importantly, the AC-DC circuit may explain how segmentation of the developing embryo in long germ-band insects such as *Drosophila*, where all segments are determined simultaneously, could have evolved from short germ-band insects, where oscillations establish the segments sequentially

(Clark, 2017). Our synthetic GRNs illustrate that it is indeed straight forward to transition between stripe-forming and oscillatory networks.

More generally, epistasis is studied extensively in different biological systems across scales (Domingo et al., 2019) because it profoundly hampers our understanding of how GRNs respond to mutations. So far, most work on the mechanistic causes of epistasis in GRNs has been purely computational (Azevedo et al., 2006; Cotterell and Sharpe, 2013; Gjuvsland et al., 2007; Omholt et al., 2000). These studies suggest that epistasis is common in GRNs and that it relies on nonlinear mechanisms of gene regulation, e.g. those generated by mutual repressions and feedbacks. Because experimental validation of these predictions is largely missing, mainly due to the high complexity of natural GRNs, our results underscore that small, mechanistically well-understood synthetic GRNs are promising model systems to study mechanisms and prevalence of epistasis (New and Lehner, 2019; Schaefer et al., 2018). The epistatic relation between GRNs 2c.6 and 3.2 also exemplifies how hybrid incompatibilities could arise: certain crossings between individuals carrying these GRNs could lead to GRNs without a stripe phenotype. This is consistent with system drift being an important source of hybrid incompatibilities that cause reproductive isolation (Johnson and Porter, 2000, 2001; Khatri and Goldstein, 2019).

Overall, we demonstrated that building many synthetic counterparts of natural systems, combined with realistic mathematical models to explore complete GP maps, can provide us both with general principles and specific insights into GRN evolution and function. We therefore anticipate that synthetic biology will gain further relevance in deciphering the mechanisms of molecular evolution.

Methods

GRN construction.

Genes encoding sfGFP, mKO2, mKate2, mCherry, mCitrine, Cerulean, Csy4 and dCas9 were obtained as previously described (Santos-Moreno and Schaeerli, 2019a; Santos-Moreno et al., 2020). All reporters were fused to orthogonal degradation tags (Butzin and Mather, 2018), as follows: mKO2-MarA, sfGFP-MarAn20, RepA70-mKate2, mCherry-MarA, mCitrine-MarAn20, RepA70-Cerulean. Primers were purchased desalted from Microsynth or Sigma-Aldrich. The GRNs were constructed employing a previously described Gibson-based cloning framework that allows for the fast and modular cloning of synthetic gene networks (Santos-Moreno and Schaeerli, 2019a). Briefly, the method consists of two steps: step 1 involves Gibson assembly of transcriptional units into individual intermediate plasmids; in step 2, these plasmids are digested with restriction enzymes so that the resulting flanking regions contain overlaps that drive a second Gibson assembly into a single plasmid to yield the final GRN. For step 1, all DNA parts carried the same Prefix (CAGCCTGCGGTCCGG) and Suffix (TCGCTGGGACGCCCG) sequences for modular Gibson assembly using MODAL (Casini et al., 2014). Basically, forward and reverse primers annealing to Prefix and Suffix sequences, respectively, were used for PCRs that added unique linkers to the DNA parts. PCR amplifications were column-purified using the Monarch PCR & DNA Cleanup Kit (NEB), and assembled using NEBuilder HiFi DNA Assembly Master Mix (NEB, 1 h 50° C) into backbones previously digested with corresponding restriction enzymes (NEB, 1 h 37° C) to yield intermediate plasmids containing individual transcriptional units. In step 2, these intermediate plasmids were digested with enzyme sets yielding overlapping sequences, purified and assembled as described above. 1 µl of non-purified Gibson reaction was transformed into 50 µl of electrocompetent NEB5a cells, and 2/5 of them were plated onto selective agar plates. Plasmids used in this study are listed in (**Supplementary Table 1**) and all sequences are provided in a supplementary file (**Data S2**).

Microplate reader experiments.

Gene expression of fluorescent reporters was used to assess synthetic GRN performance; fluorescence was measured in microplate readers (except for the microfluidic experiments in **Fig. 7**). MK01 (Kogenaru and Tans, 2014) electrocompetent cells were transformed with a “constant” plasmid encoding proteins required for GRN function (namely dCas9 and Csy4) (Santos-Moreno and Schaeerli, 2019a) as well as with a “variable” vector bearing AraC (when needed) and the CRISPRi GRN (see **Supplementary Table 1**). 2 ml of selective LB were inoculated with single colonies and incubated at 37° C for ~6 h with 200 rpm shaking; cells were pelleted at 4000 rcf and resuspended in selective EZ medium (Teknova) containing 0.4% glycerol. 120 µl of 0.05 OD₆₀₀

bacterial suspensions were added per well on a 96-well CytoOne plate (Starlab), and 2.4 μ l of L-arabinose (Sigma) were added to yield the indicated concentrations. Plates were incubated at 37° C with double-orbital shaking in a Synergy H1 microplate reader (Bioteck) running Gen5 3.04 software. Fluorescence was determined after ~16 h with the following settings: mKO2: Ex. 542 nm, Em. 571 nm; sfGPF: Ex. 479 nm, Em. 520 nm; mKate2: Ex. 588 nm, Em. 633 nm. Fluorescence levels were treated as follows: i) the fluorescence signal in a blank sample was subtracted, ii) the resulting value was divided by the absorbance at 600 nm to correct for differences in bacterial concentration, and finally iii) the bacterial auto-fluorescence of a strain with no reporter genes was subtracted. Subsequently, corrected fluorescence was normalized to a percentage scale by dividing all values of a given color by the highest value of that color. Normalized data were plotted in R (R Core Team, 2017) using RStudio 1.0.143 (running R 3.4.0). Source data are provided in a supplementary file (**Data S3**).

Microfluidic experiments.

MK01 (Kogenaru and Tans, 2014) electrocompetent cells were transformed with the constant plasmid pJ1996_v2 (Santos-Moreno and Schaeferli, 2019a) and a variable plasmid encoding a CRISPRi GRN. Single colonies were used to inoculate 5 ml of selective LB, which were grown overnight at 37° C. Next morning, 3 ml of selective EZ containing 0.85 g l⁻¹ Pluronic F-127 (Sigma) were inoculated with the overnight preculture in a 1:100 ratio and grown for 3-4 h at 37° C. Cells were centrifuged for 10 min at 4000 rcf and resuspended in ~10 μ l of the supernatant to obtain a dense suspension, which was loaded into the PDMS microfluidics device. Cells were grown in a continuous culture inside microfluidic chambers (dimensions: 1.2 μ m x 12 μ m x 60 μ m, h x w x l, purchased from Wunderlichips) (Santos-Moreno et al., 2020) for 2 days with a constant 0.5 ml h⁻¹ supply of fresh medium (selective EZ plus 0.85 g l⁻¹ Pluronic F-127) and removal of waste and excess of bacteria, powered by an AL-300 pump (World Precision Instruments). For GRNs 2-OS.1, 1-OS.1 and 1-OS.2 the overnight and the subsequent 1:100 incubations contained 0.2% Ara, while 0.0001% Ara (for 2-OS.1) or 0.2% Ara (for 1-OS.1 and 1-OS.2) were used in the medium for the microfluidic experiment. For 1-OS.3, which lacks the P_{BAD} promoter, no Ara was used in any of the media. Imaging was performed using a Leica DMi8 microscope and a Leica DFC9000 GT camera controlled by the Leica Application Suite X 3.4.2.18368, with the following settings: Cerulean: Ex. 440 nm 10% 50 ms, Em. 457-483 nm; mCitrine: Ex. 510 nm 10% 50 ms, Em. 520-550 nm; mCherry: Ex. 550 nm 20% 200 ms, Em. 600-670 nm; sfGFP: Ex. 470 nm 30% 200 ms, Em. 507-543 nm; mKO2 and mKate2 (indistinguishable): Ex. 550 nm 30% 200 ms, Em. 520-550 nm. Images were acquired every 10 min with LAS X software, and analyzed using Fiji (Schindelin et al., 2012) for montage. Normalized data were plotted in R (R Core Team, 2017) using RStudio 1.0.143 (R 3.4.0).

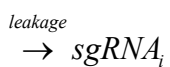
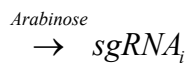
Mathematical modeling, overview.

We developed an ensemble of mechanistic mathematical models that capture in detail level the biology of the transcription/translation/fluorescent maturation of various 2-node and 3-node GRNs. A model can be automatically generated depending on the GRN we want to simulate. Below, we decompose the model into its two core structures and assumptions. Next, we continue with additional functions we utilize to account for cell growth in the experiments.

Modeling the dynamics of sgRNAs.

The production rate of the sgRNA(s) depends on having either an inducible promoter (by arabinose) or a constitutively expressed promoter. The orange node (see **Fig. 3**) is always induced by arabinose; the other two nodes (green and blue) have a constitutively expressed promoter. We also considered in our model the leakage of sgRNA(s) by the inducible promoter. The sgRNA(s) can bind reversibly to the catalytically-dead mutant dCas, which forms a complex sgRNA:dCas. In turn, the sgRNA:dCas complex can bind reversibly and inhibit, via its target sequence on the promoter (DNA), the respective gene expression, forming a sgRNA:dCas:DNA complex. We assume that RNAases act on degrading the sgRNA(s), whereas the complexes are affected by the dilution rate, m (see below for details on dilution). These biomolecular processes are described as chemical reactions.

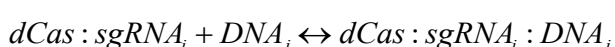
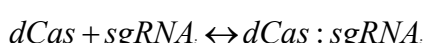
Two chemical reactions represent the induction by arabinose and the leakage that specific promoter has



and one chemical reaction depicts the case of the constitutive promoter:



where the number of sgRNAs that is available is indicated with i and j , taking values from one to three based on the three reporter protein-coding genes that exist in the GRNs. RNA degradation (denoted by the empty symbol) as well as complex formation with dCas and DNA are modeled as:



Since the plasmid containing dCas is constitutively expressed, the total concentration of dCas is conserved. The total promoter concentration (DNA_j) is also conserved. These assumptions lead to the algebraic equations (using square brackets to denote concentrations):

$$[dCas_{total}] = [dCas] + \sum_i [dCas : sgRNA_i] + \sum_{i,j} [dCas : sgRNA_i : DNA_j]$$

$$[DNA_{total,j}] = [DNA_j] + [dCas : sgRNA_i : DNA_j].$$

By using mass action kinetics (except for inducible promoters and dilution, see below), we transform the above chemical reactions and assumptions into a system of ordinary differential equations (ODEs):

$$\frac{d[sgRNA_i]}{dt} = f_{(Ara)} + b_{sgRNA_i} - d_{RNA} \cdot [sgRNA_i]$$

$$\frac{d[sgRNA_i]}{dt} = k_{sgRNA_i} \cdot [DNA_j] - d_{RNA} \cdot [sgRNA_i]$$

$$\frac{d[dCas : sgRNA_i]}{dt} = k_{f_{ds}} \cdot [dCas] \cdot [sgRNA_i] + k_{r_{dsd}} \cdot [dCas : sgRNA_i : DNA_j]$$

$$-m \cdot [dCas : sgRNA_i] - k_{r_{ds}} \cdot [dCas : sgRNA_i] - k_{f_{dsd}} \cdot [dCas : sgRNA_i] \cdot [DNA_j]$$

$$\frac{d[dCas : sgRNA_i : DNA_j]}{dt} = k_{f_{dsd}} \cdot [dCas : sgRNA_i] \cdot [DNA_j] - k_{r_{dsd}} \cdot [dCas : sgRNA_i : DNA_j]$$

$$-m \cdot [dCas : sgRNA_i : DNA_j]$$

Depending on whether the sgRNA is expressed by an inducible or a constitutive promoter, we use either the first or the second ODE. If there is an inducible promoter, then promoter leakage is constant, b_{sgRNA_i} . Production and degradation kinetic constants are k_{sgRNA_i} and d_{RNA} ; the binding and unbinding constants of sgRNA-dCas and sgRNA-dCas-DNA complexes are $k_{f_{ds}}$, $k_{r_{ds}}$ and $k_{f_{dsd}}$, $k_{r_{dsd}}$, respectively.

In addition, we assume a Hill function for promoter induction by arabinose (Ara):

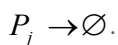
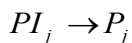
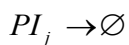
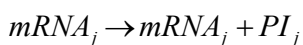
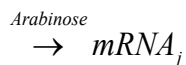
$$f_{(Ara_{sgRNA_i})} = \frac{Ara^n}{Ara^n + K_m^n} \cdot k_2 \cdot [DNA_{total,j}] \cdot (1 - b_{sgRNA_i}),$$

where n is the Hill coefficient, K_m is the affinity constant and k_2 is the production constant.

Dynamics of reporter protein coding genes.

Similar to the production rate of sgRNAs, the mRNA production of the three reporters used in this study depends either on the activity of an inducible promoter or on a constitutive promoter (expression of orange node via arabinose induction, green and blue node via constitutive

promoter). mRNA translation produces protein PI_j , which matures to the final fluorescent reporter (P_j). mRNA is degraded by the same rate as the degradation of sgRNAs. However, the reporter proteins (immature and fluorescent) undergo active degradation (which depends on the reporter) and dilution (see growth model section). The chemical reactions that summarize the expression of the reporter proteins are:



Again, we differentiate between arabinose-inducible and constitutive promoters and account for leakage. By assuming mass-action kinetics, the ODE system is:

$$\frac{d[mRNA_j]}{dt} = f_{(Ara_{mRNA_j})} + b_{mRNA_j} - d_{RNA} \cdot [mRNA_j]$$

$$\frac{d[mRNA_j]}{dt} = k_{mRNA_j} \cdot [DNA_j] - d_{RNA} \cdot [mRNA_j]$$

$$\frac{d[PI_j]}{dt} = k_{PI_j} \cdot [mRNA_j] - m_{PI_j} \cdot [PI_j] - (m + d_{PI_j}) \cdot [PI_j]$$

$$\frac{d[P_j]}{dt} = m_{PI_j} \cdot [PI_j] - (m + d_{PI_j}) \cdot [P_j]$$

Kinetic constants of production, degradation and promoter leakage are k_{mRNA_j} , d_{RNA} and b_{sgRNA_i} . Translation, maturation and active degradation constants are k_{PI_j} , m_{PI_j} and d_{PI_j} respectively. In addition, $f_{(Ara_{mRNA_j})}$ is the same function as above, but for $mRNA_j$:

$$f_{(Ara_{mRNA_j})} = \frac{Ara^n}{Ara^n + K_m^n} \cdot k_2 \cdot [DNA_{total,j}] \cdot (1 - b_{mRNA_j}).$$

Growth model.

We represent the cell population growth during the microplate experiment, $G(t)$, by a superposition of three generalized logistic functions. This approach allows capturing events such as diauxic shifts in which growth slows down due to limited nutrient availability. Specifically:

$$G(t) = p_1 + \sum_{k=1}^3 \frac{p_2^k}{\left(1 + p_3^k e^{-t \cdot p_4^k}\right)^{p_5^k}}.$$

In our model, the dilution rate m is the derivative of $G(t)$ with parameters estimated from the appropriate data (see **Data S1**). The rest of the experimental data was used for independent model validation.

Promoter efficiencies.

The P_H (BBa_J23100) and P_M (BBa_J23102) promoters that were used for building some of the synthetic GRNs are from a standard collection recovered from a library screen (Anderson et al., 2010). Therefore, in our modelling process we used the measured strength 1 and 0.86, respectively. Concerning the P_L (BBa_J23150) promoter, we found discrepancies between previously determined promoter strengths (Davis et al., 2011; Kelly et al., 2009) and our estimates, possibly due to context dependent effects on gene expression (Karamasioti et al., 2017). Specifically, we identified common promoters (BBa_J23102, BBa_J23116, BBa_J23113) in the dataset from Kelly et al. and the Anderson collection. Using linear regression, we predicted the promoter efficiency of the P_L we would have observed if it had been measured in the Anderson collection. With the same procedure, we compared the Davis dataset and the Anderson collection (common promoters: BBa_J23101, BBa_J23113). For the two comparisons, we predicted for the P_L promoter a relative strength of 0.3 and 0.2, respectively. However, from our estimation we predicted that the strength was 0.75. Given that we have the additional control analysis which contains the relative strengths identified by (Davis et al., 2011; Kelly et al., 2009), we continued with our estimated strength when comparing to the experimental data.

Translation of mRNA induced by arabinose.

The expression of the orange node (reporter protein: mKO2) is induced by arabinose, controlling the expression of the mKO2 mRNA, which then translates into the immature protein of mKO2. When calibrating the mathematical models we noticed non-linearities in the arabinose response, although we used the MK01 strain (Kogenaru and Tans, 2014). A possible explanation (Megerle et al., 2008) is the difference in the number of transporters per cell in the population; cells can accumulate sufficient arabinose (or not) to overcome the internal threshold concentration for gene activation. We tackled this observation phenomenologically by making the translation constant dependent on the concentration of arabinose, independent of the modeled topologies.

Scaling parameters and measurement models.

To map the model output (P_A , P_B , P_C) to the microplate reader experiments, we included three scaling factors (for the three fluorescent reporters) in the optimization procedure (**Data S1**). Given that the experiment for each reporter was performed with the same settings, we assumed three measurement models. We performed linear regression on the variance (s.d.) as a function of average fluorescent signal per reporter. We used the following models per reporter, with its average fluorescent signal x (**Fig. S5**):

$$GFP(x) = \begin{cases} 10350, & x < 7e+04 \\ 0.13 \cdot x + 1250, & 7e+04 \leq x \leq 2.5e+05 \\ 3.375e+04, & x > 2.5e+05 \end{cases},$$

$$mKO2(x) = \begin{cases} 899, & x < 600 \\ 0.08 \cdot x + 419, & 6e+03 \leq x \leq 2e+04 \\ 2e+03, & x > 2e+04 \end{cases}, \text{ and}$$

$$mKate2(x) = \begin{cases} 43, & x < 500 \\ 0.03 \cdot x + 23, & x \geq 500 \end{cases}.$$

Definition of a stripe.

To characterize a GRN as a stripe-forming one, initially we normalized the simulated data. We divided each reporter model output (P_A , P_B , P_C) at 900 min for the different arabinose concentrations by the maximum observed for each reporter (at 900 min for the same arabinose concentrations). Next, we identified the node that reached maximum peak (i.e. a value of 1) when the other two were at the minimum. To accept or reject a stripe (even if a node was identified), we set a threshold of 6% increase and decrease, concerning the average of two lower and two higher arabinose induction levels with respect to the maximum point. Therefore, a functional (BLUE- or GREEN-stripe) phenotype should on average at the two lowest and two highest arabinose concentrations have at least an increase of 6% and a decrease of 6%. We designated all other phenotypes as non-functional.

Mutational change in GRNs.

Within the modeling framework, we represent each GRN as an 8-length vector. The first six elements of the vector represent the positions of an inhibition, similar to **Fig. 4E** (or absence, represented with 0). In the genotype networks, we define one mutational change as the 1-Hamming distance between any one changes in the 8-length vectors (ie 1-neighborhood).

Genotype maps of synthetic GRNs.

We created genotype maps by finding all the possible combinations of the modular parts at our disposal (i.e. qualitative and quantitative changes) and evaluating them for observing a non-functional or functional phenotype. A single set of parameters (that best minimizes the objective function) was used for all the forward simulations. Specifically, we had: 1) four different promoter efficiencies (the P_L, P_M, P_H and the 0 case) with two available promoter positions (green and blue node), 2) six sgRNAs, and 3) 42 topologies with a minimum of three and a maximum of six inhibitions. Therefore, for each topology the total number of GRNs is:

$$T_{(E)} = p^2 \cdot s^E,$$

where p is the total number of promoter efficiencies, s is the total number of sgRNAs, and E depends on the number of total inhibitions a specific topology has. For the control analysis with artificial parameter values (a regular grid in parameter space), the number of modular parts consisted of: 1) five evenly spaced (from 0 to 1) promoter efficiencies with two available promoter positions (green and blue node), 2) five sgRNAs with evenly spaced kinetic dissociation constants (from 5 to 45 nM), and 3) 42 topologies.

Connectivity of genotype networks.

A connected component of an undirected graph is the maximal set of nodes such that each pair of nodes is connected by a path (Wilson, 2009). To evaluate the connectivity for the genotype networks, we utilized the command *components* from the *igraph* package (Csárdi and Nepusz, 2006) in Rstudio (RStudio Team, 2020). It uses either a simple breadth-first search or two consecutive depth-first searches.

Robustness per perturbation.

As in (Catalán et al., 2018), we measured the fraction of neighbors that maintain the same phenotype per perturbation (i.e. changes in sgRNAs or in promoter efficiencies), termed here as robustness per perturbation (or neutrality, see (Catalán et al., 2018)). We randomly sampled 1% of GRNs per functional phenotypes (2000 GRNs) and 0.1% of non-functional phenotype (2000 GRNs) and evaluated all their neighbors (which accounts for ~4.5% of the total possible GRNs).

Random walks.

To determine the path length for alternating phenotypes (GREEN-stripe, BLUE-stripe and NF phenotypes), we randomly selected 5% GRNs per functional phenotype and 2% for the non-functional one (~10700 GRNs with BLUE-stripe and GREEN-stripe, and 28903 GRNs for NF).

From these starting GRNs, the algorithm proceeded by uniform random selection of a GRN from the set of neighboring GRNs. We stopped the walk upon a change in phenotype or when the maximum number of steps (50 for functional phenotypes, 300 for NF) was reached. We used the built-in command *random_walk* from the *igraph* package (Csárdi and Nepusz, 2006) in Rstudio (RStudio Team, 2020).

Prevalence of epistasis.

To measure the occurrence of epistasis within our genotype networks we sampled again 5% GRNs per functional phenotype and 2% for the non-functional one. Our goal was for each sampled GRN to evaluate if it is part of an orthogonal network of GRNs, in which only one of the direct neighbors will differ in the phenotype. We did this by evaluating the 1- and 2-Hamming distance neighborhoods of the sampled GRN.

Data availability

Source data of experiments are provided in **Data S3**.

All sequences are provided in **Data S2**.

The model related datasets generated during and/or analyzed are available at GitHub. Model parameters and relative information are provided in **Data S1**.

Code availability

Custom code for the analysis and generation of model related figures is available at GitHub.

Author Contributions

J.S.M. and Y.S. designed the experimental research. J.S.M. and H.K. performed experiments and analyzed data. E.T. and J.S. designed the computational part and performed the mathematical modeling. J.S.M., Y.S., E.T., and J.S. wrote the manuscript. All authors revised the manuscript and approved the final version of the manuscript.

Conflict of Interest

The authors declare no conflict of interest.

Acknowledgments

We thank Clement Gallay and Jan-Willem Veening for help with microscopy, Ruben Pérez-Carrasco and Björn Vessman for exploratory CRISPRi stripe models, and Joshua Payne and Berta Verd for useful feedback on a previous version of the manuscript. We also thank Mariapia Chindamo, Aysun El Wardani, Florence Gauye, Virginie Kahabedian, Borany Kim, Léo Moser, Antoine Triani and Lucie Gilliéron for help with cloning, and all Schaerli lab members for useful discussions. This work was funded in part by the Swiss National Science Foundation (grants 31003A_175608 and 310030_200532 awarded to Y.S).

References

Aguilar-Rodríguez, J., Peel, L., Stella, M., Wagner, A., and Payne, J.L. (2018). The architecture of an empirical genotype-phenotype map. *Evolution* 72, 1242-1260.

Aguirre, J., Catalán, P., Cuesta, J.A., and Manrubia, S. (2018). On the networked architecture of genotype spaces and its critical effects on molecular evolution. *Open Biology* 8, 180069.

Ahnert, S.E. (2017). Structural properties of genotype–phenotype maps. *Journal of The Royal Society Interface* 14, 20170275.

Alon, U. (2006). An Introduction to Systems Biology: Design Principles of Biological Circuits (Chapman and Hall/CRC).

Alon, U. (2007). Network motifs: theory and experimental approaches. *Nature Reviews Genetics* 8, 450-461.

Anderson, D.W., McKeown, A.N., and Thornton, J.W. (2015). Intermolecular epistasis shaped the function and evolution of an ancient transcription factor and its DNA binding sites. *eLife* 4, e07864.

Anderson, J., Dueber, J.E., Leguia, M., Wu, G.C., Goler, J.A., Arkin, A.P., and Keasling, J.D. (2010). BglBricks: A flexible standard for biological part assembly. *Journal of Biological Engineering* 4, 1.

Arboleda-Rivera, J.C., Machado-Rodríguez, G., Rodríguez, B.A., and Gutiérrez, J. (2022). Elucidating multi-input processing 3-node gene regulatory network topologies capable of generating striped gene expression patterns. *PLOS Computational Biology* 18, e1009704.

Azevedo, R.B.R., Lohaus, R., Srinivasan, S., Dang, K.K., and Burch, C.L. (2006). Sexual reproduction selects for robustness and negative epistasis in artificial gene networks. *Nature* 440, 87-90.

Baier, F., Hong, N., Yang, G., Pabis, A., Miton, C.M., Barrozo, A., Carr, P.D., Kamerlin, S.C.L., Jackson, C.J., and Tokuriki, N. (2019). Cryptic genetic variation shapes the adaptive evolutionary potential of enzymes. *eLife* 8, e40789.

Baier, F., and Schaefer, Y. (2021). Addressing Evolutionary Questions with Synthetic Biology. In *Evolutionary Systems Biology: Advances, Questions, and Opportunities*, A. Crombach, ed. (Cham: Springer International Publishing), pp. 135-157.

Balaskas, N., Ribeiro, A., Panovska, J., Dessaad, E., Sasai, N., Page, K.M., Briscoe, J., and Ribes, V. (2012). Gene regulatory logic for reading the Sonic Hedgehog signaling gradient in the vertebrate neural tube. *Cell* 148, 273-284.

Bayer, T.S. (2010). Using Synthetic Biology to Understand the Evolution of Gene Expression. *Current Biology* 20, R772-R779.

Bendixsen, D.P., Collet, J., Østman, B., and Hayden, E.J. (2019). Genotype network intersections promote evolutionary innovation. *PLOS Biology* 17, e3000300.

Bershteyn, S., Goldin, K., and Tawfik, D.S. (2008). Intense Neutral Drifts Yield Robust and Evolvable Consensus Proteins. *Journal of Molecular Biology* 379, 1029-1044.

Bloom, J.D., Romero, P.A., Lu, Z., and Arnold, F.H. (2007). Neutral genetic drift can alter promiscuous protein functions, potentially aiding functional evolution. *Biology Direct* 2, 17.

Butzin, N.C., and Mather, W.H. (2018). Crosstalk between Diverse Synthetic Protein Degradation Tags in *Escherichia coli*. *ACS Synthetic Biology* 7, 54-62.

Casini, A., MacDonald, J.T., De Jonghe, J., Christodoulou, G., Freemont, P.S., Baldwin, G.S., and Ellis, T. (2014). One-pot DNA construction for synthetic biology: the Modular Overlap-Directed Assembly with Linkers (MODAL) strategy. *Nucleic Acids Research* 42, e7.

Catalán, P., Wagner, A., Manrubia, S., and Cuesta, J.A. (2018). Adding levels of complexity enhances robustness and evolvability in a multilevel genotype–phenotype map. *Journal of The Royal Society Interface* 15, 20170516.

Chau, A.H., Walter, J.M., Gerardin, J., Tang, C., and Lim, W.A. (2012). Designing synthetic regulatory networks capable of self-organizing cell polarization. *Cell* 151, 320-332.

Ciliberti, S., Martin, O.C., and Wagner, A. (2007a). Innovation and robustness in complex regulatory gene networks. *Proceedings of the National Academy of Sciences* 104, 13591.

Ciliberti, S., Martin, O.C., and Wagner, A. (2007b). Robustness Can Evolve Gradually in Complex Regulatory Gene Networks with Varying Topology. *PLOS Computational Biology* 3, e15.

Clark, E. (2017). Dynamic patterning by the *Drosophila* pair-rule network reconciles long-germ and short-germ segmentation. *PLOS Biology* 15, e2002439.

Cotterell, J., and Sharpe, J. (2010). An atlas of gene regulatory networks reveals multiple three-gene mechanisms for interpreting morphogen gradients. *Molecular Systems Biology* 6, 425.

Cotterell, J., and Sharpe, J. (2013). Mechanistic Explanations for Restricted Evolutionary Paths That Emerge from Gene Regulatory Networks. *PLOS ONE* 8, e61178.

Crocker, J., and Ilsley, G.R. (2017). Using synthetic biology to study gene regulatory evolution. *Current Opinion in Genetics & Development* 47, 91-101.

Crombach, A., Wotton, K.R., Jiménez-Guri, E., and Jaeger, J. (2016). Gap Gene Regulatory Dynamics Evolve along a Genotype Network. *Molecular Biology and Evolution* 33, 1293-1307.

Csárdi, G., and Nepusz, T. (2006). The igraph software package for complex network research. *InterJournal Complex Systems*, 1695.

Dalal, C.K., and Johnson, A.D. (2017). How transcription circuits explore alternative architectures while maintaining overall circuit output. *Genes & Development* 31, 1397-1405.

Davis, J.H., Rubin, A.J., and Sauer, R.T. (2011). Design, construction and characterization of a set of insulated bacterial promoters. *Nucleic Acids Research* 39, 1131-1141.

Domingo, J., Baeza-Centurion, P., and Lehner, B. (2019). The Causes and Consequences of Genetic Interactions (Epistasis). *Annual Review of Genomics and Human Genetics* 20, 433-460.

Egea, J.A., Henriques, D., Cokelaer, T., Villaverde, A.F., MacNamara, A., Danciu, D.-P., Banga, J.R., and Saez-Rodriguez, J. (2014). MEIGO: an open-source software suite based on metaheuristics for global optimization in systems biology and bioinformatics. *BMC bioinformatics* 15, 1-9.

Elowitz, M.B., and Leibler, S. (2000). A synthetic oscillatory network of transcriptional regulators. *Nature* 403, 335-338.

Espah Borujeni, A., Zhang, J., Doosthosseini, H., Nielsen, A.A.K., and Voigt, C.A. (2020). Genetic circuit characterization by inferring RNA polymerase movement and ribosome usage. *Nature Communications* 11, 5001.

Ewe, C.K., Torres Cleuren, Y.N., and Rothman, J.H. (2020). Evolution and Developmental System Drift in the Endoderm Gene Regulatory Network of *Caenorhabditis* and Other Nematodes. *Frontiers in Cell and Developmental Biology* 8, 150.

Floc'hlay, S., Wong, E.S., Zhao, B., Viales, R.R., Thomas-Chollier, M., Thieffry, D., Garfield, D.A., and Furlong, E.E.M. (2021). Cis-acting variation is common across regulatory layers but is often buffered during embryonic development. *Genome Research* 31, 211-224.

Friedlander, T., Prizak, R., Barton, N.H., and Tkačik, G. (2017). Evolution of new regulatory functions on biophysically realistic fitness landscapes. *Nature Communications* 8, 216.

Gjuvsland, A.B., Hayes, B.J., Omholt, S.W., and Carlborg, O.r. (2007). Statistical Epistasis Is a Generic Feature of Gene Regulatory Networks. *Genetics* 175, 411-420.

Goldstein, R.A. (2008). The structure of protein evolution and the evolution of protein structure. *Current Opinion in Structural Biology* 18, 170-177.

Goltsev, Y., Hsiong, W., Lanzaro, G., and Levine, M. (2004). Different combinations of gap repressors for common stripes in *Anopheles* and *Drosophila* embryos. *Developmental Biology* 275, 435-446.

Haag, E.S. (2014). The Same but Different: Worms Reveal the Pervasiveness of Developmental System Drift. *PLOS Genetics* 10, e1004150.

Hayden, E.J., Ferrada, E., and Wagner, A. (2011). Cryptic genetic variation promotes rapid evolutionary adaptation in an RNA enzyme. *Nature* 474, 92-95.

Hinman, V.F., and Davidson, E.H. (2007). Evolutionary plasticity of developmental gene regulatory network architecture. *Proceedings of the National Academy of Sciences* 104, 19404-19409.

Igler, C., Lagator, M., Tkačik, G., Bollback, J.P., and Guet, C.C. (2018). Evolutionary potential of transcription factors for gene regulatory rewiring. *Nature Ecology & Evolution* 2, 1633-1643.

Isalan, M., Lemerle, C., Michalodimitrakis, K., Horn, C., Beltrao, P., Rainieri, E., Garriga-Canut, M., and Serrano, L. (2008). Evolvability and hierarchy in rewired bacterial gene networks. *Nature* 452, 840-845.

Jaeger, J. (2011). The gap gene network. *Cellular and Molecular Life Sciences* 68, 243-274.

Jaeger, J. (2018). Shift happens: The developmental and evolutionary dynamics of the gap gene system. *Current Opinion in Systems Biology* 11, 65-73.

Jimenez, A., Cotterell, J., Munteanu, A., and Sharpe, J. (2015). Dynamics of gene circuits shapes evolvability. *Proceedings of the National Academy of Sciences* 112, E5110.

Johnson, A.D. (2017). The rewiring of transcription circuits in evolution. *Current Opinion in Genetics & Development* 47, 121-127.

Johnson, N.A., and Porter, A.H. (2000). Rapid Speciation via Parallel, Directional Selection on Regulatory Genetic Pathways. *Journal of Theoretical Biology* 205, 527-542.

Johnson, N.A., and Porter, A.H. (2001). Toward a new synthesis: population genetics and evolutionary developmental biology. *Genetica* 112, 45-58.

Jones, D.L., Leroy, P., Unoson, C., Fange, D., Curic, V., Lawson, M.J., and Elf, J. (2017). Kinetics of dCas9 target search in *Escherichia coli*. *Science* 357, 1420-1423.

Karamasioti, E., Lormeau, C., and Stelling, J. (2017). Computational design of biological circuits: putting parts into context. *Molecular Systems Design & Engineering* 2, 410-421.

Karlebach, G., and Shamir, R. (2008). Modelling and analysis of gene regulatory networks. *Nature Reviews Molecular Cell Biology* 9, 770-780.

Kelly, J.R., Rubin, A.J., Davis, J.H., Ajo-Franklin, C.M., Cumbers, J., Czar, M.J., de Mora, K., Glieberman, A.L., Monie, D.D., and Endy, D. (2009). Measuring the activity of BioBrick promoters using an in vivo reference standard. *Journal of Biological Engineering* 3, 4.

Khatri, B.S., and Goldstein, R.A. (2019). Biophysics and population size constrains speciation in an evolutionary model of developmental system drift. *PLOS Computational Biology* 15, e1007177.

Kiontke, K., Barrière, A., Kolotuev, I., Podbilewicz, B., Sommer, R., Fitch, D.H.A., and Félix, M.-A. (2007). Trends, Stasis, and Drift in the Evolution of Nematode Vulva Development. *Current Biology* 17, 1925-1937.

Kogenaru, M., and Tans, S.J. (2014). An improved *Escherichia coli* strain to host gene regulatory networks involving both the AraC and LacI inducible transcription factors. *Journal of Biological Engineering* 8, 2.

Lagator, M., Sarikas, S., Acar, H., Bollback, J.P., and Guet, C.C. (2017). Regulatory network structure determines patterns of intermolecular epistasis. *eLife* 6, e28921.

Li, W., Krishna, S., Pigolotti, S., Mitarai, N., and Jensen, M.H. (2012). Switching between oscillations and homeostasis in competing negative and positive feedback motifs. *Journal of Theoretical Biology* 307, 205-210.

Lipman, D.J., Wilbur, W.J., and Smith, J.M. (1991). Modelling neutral and selective evolution of protein folding. *Proceedings of the Royal Society of London Series B: Biological Sciences* 245, 7-11.

Martchenko, M., Levitin, A., Hogues, H., Nantel, A., and Whiteway, M. (2007). Transcriptional Rewiring of Fungal Galactose-Metabolism Circuitry. *Current Biology* 17, 1007-1013.

Maynard Smith, J. (1970). Natural Selection and the Concept of a Protein Space. *Nature* 225, 563-564.

Megerle, J.A., Fritz, G., Gerland, U., Jung, K., and Rädler, J.O. (2008). Timing and Dynamics of Single Cell Gene Expression in the Arabinose Utilization System. *Biophysical Journal* 95, 2103-2115.

Munteanu, A., Cotterell, J., Sole, R.V., and Sharpe, J. (2014). Design principles of stripe-forming motifs: the role of positive feedback. *Scientific Reports* 4, 5003.

New, A.M., and Lehner, B. (2019). Harmonious genetic combinations rewire regulatory networks and flip gene essentiality. *Nature Communications* 10, 3657.

Nguyen Ba, A.N., Lawrence, K.R., Rego-Costa, A., Gopalakrishnan, S., Temko, D., Michor, F., and Desai, M.M. (2022). Barcoded bulk QTL mapping reveals highly polygenic and epistatic architecture of complex traits in yeast. *eLife* 11, e73983.

Nocedal, I., Mancera, E., and Johnson, A.D. (2017). Gene regulatory network plasticity predates a switch in function of a conserved transcription regulator. *eLife* 6, e23250.

Omholt, S.W., Plahte, E., Øyehaug, L., and Xiang, K. (2000). Gene Regulatory Networks Generating the Phenomena of Additivity, Dominance and Epistasis. *Genetics* 155, 969-980.

Panovska-Griffiths, J., Page, K.M., and Briscoe, J. (2013). A gene regulatory motif that generates oscillatory or multiway switch outputs. *Journal of the Royal Society Interface* 10, 20120826.

Payne, J.L., Khalid, F., and Wagner, A. (2018). RNA-mediated gene regulation is less evolvable than transcriptional regulation. *Proceedings of the National Academy of Sciences* 115, E3481-E3490.

Payne, J.L., Moore, J.H., and Wagner, A. (2014). Robustness, Evolvability, and the Logic of Genetic Regulation. *Artificial Life* 20, 111-126.

Payne, J.L., and Wagner, A. (2013). Constraint and Contingency in Multifunctional Gene Regulatory Circuits. *PLOS Computational Biology* 9, e1003071.

Payne, J.L., and Wagner, A. (2014). The Robustness and Evolvability of Transcription Factor Binding Sites. *Science* 343, 875-877.

Payne, J.L., and Wagner, A. (2015). Mechanisms of mutational robustness in transcriptional regulation. *Frontiers in Genetics* 6.

Payne, J.L., and Wagner, A. (2019). The causes of evolvability and their evolution. *Nature Reviews Genetics* 20, 24-38.

Perez-Carrasco, R., Barnes, C.P., Schaerli, Y., Isalan, M., Briscoe, J., and Page, K.M. (2018). Combining a Toggle Switch and a Repressilator within the AC-DC Circuit Generates Distinct Dynamical Behaviors. *Cell Systems* 6, 521-530.

Podgornaia, A.I., and Laub, M.T. (2015). Pervasive degeneracy and epistasis in a protein-protein interface. *Science* 347, 673.

Ptashne, M., and Gann, A. (2002). *Genes & Signals* (Cold Spring Harbor Laboratory Press).

R Core Team (2017). R: A language and environment for statistical computing. R Foundation for Statistical Computing, Vienna, Austria.

Rogers, K.W., and Schier, A.F. (2011). Morphogen Gradients: From Generation to Interpretation. *Annual Review of Cell and Developmental Biology* 27, 377-407.

RStudio Team (2020). RStudio: Integrated Development for R. RStudio, PBC, Boston, MA

Sagner, A., and Briscoe, J. (2017). Morphogen interpretation: concentration, time, competence, and signaling dynamics. *WIREs Developmental Biology* 6, e271.

Santos-Moreno, J., and Schaerli, Y. (2019a). A Framework for the Modular and Combinatorial Assembly of Synthetic Gene Circuits. *ACS Synthetic Biology* 8, 1691-1697.

Santos-Moreno, J., and Schaerli, Y. (2019b). Using Synthetic Biology to Engineer Spatial Patterns. *Advanced Biosystems* 3, 1800280.

Santos-Moreno, J., and Schaerli, Y. (2020). CRISPR-based gene expression control for synthetic gene circuits. *Biochemical Society Transactions* 48, 1979–1993.

Santos-Moreno, J., Tasiudi, E., Stelling, J., and Schaeerli, Y. (2020). Multistable and dynamic CRISPRi-based synthetic circuits. *Nature Communications* 11, 2746.

Schaeerli, Y., Jimenez, A., Duarte, J.M., Mihajlovic, L., Renggli, J., Isalan, M., Sharpe, J., and Wagner, A. (2018). Synthetic circuits reveal how mechanisms of gene regulatory networks constrain evolution. *Molecular Systems Biology* 14, e8102.

Schaeerli, Y., Munteanu, A., Gili, M., Cotterell, J., Sharpe, J., and Isalan, M. (2014). A unified design space of synthetic stripe-forming networks. *Nature Communications* 5, 4905.

Schindelin, J., Arganda-Carreras, I., Frise, E., Kaynig, V., Longair, M., Pietzsch, T., Preibisch, S., Rueden, C., Saalfeld, S., Schmid, B., et al. (2012). Fiji: an open-source platform for biological-image analysis. *Nature Methods* 9, 676.

Schultes, E.A., and Bartel, D.P. (2000). One Sequence, Two Ribozymes: Implications for the Emergence of New Ribozyme Folds. *Science* 289, 448.

Schuster, P., Fontana, W., Stadler, P.F., and Hofacker, I.L. (1994). From sequences to shapes and back: a case study in RNA secondary structures. *Proceedings of the Royal Society of London Series B: Biological Sciences* 255, 279-284.

Sezonov, G., Joseleau-Petit, D., and D'Ari, R. (2007). Escherichia coli Physiology in Luria-Bertani Broth. *Journal of Bacteriology* 189, 8746-8749.

Sorrells, T.R., Booth, L.N., Tuch, B.B., and Johnson, A.D. (2015). Intersecting transcription networks constrain gene regulatory evolution. *Nature* 523, 361-365.

True, J.R., and Haag, E.S. (2001). Developmental system drift and flexibility in evolutionary trajectories. *Evolution & Development* 3, 109-119.

Tsong, A.E., Tuch, B.B., Li, H., and Johnson, A.D. (2006). Evolution of alternative transcriptional circuits with identical logic. *Nature* 443, 415-420.

Verd, B., Monk, N.A.M., and Jaeger, J. (2019). Modularity, criticality, and evolvability of a developmental gene regulatory network. *eLife* 8, e42832.

Voordeckers, K., Pougach, K., and Verstrepen, K.J. (2015). How do regulatory networks evolve and expand throughout evolution? *Current Opinion in Biotechnology* 34, 180-188.

Wagner, A. (2005). *Robustness and Evolvability in Living Systems* (Princeton University Press).

Wagner, A. (2008). Robustness and evolvability: a paradox resolved. *Proceedings of the Royal Society B: Biological Sciences* 275, 91-100.

Wagner, A. (2011). The molecular origins of evolutionary innovations. *Trends in Genetics* 27, 397-410.

Wagner, A. (2012). The role of robustness in phenotypic adaptation and innovation. *Proceedings of the Royal Society of London Series B: Biological Sciences* 279, 1249-1258.

Weiss, K.M., and Fullerton, S.M. (2000). Phenogenetic Drift and the Evolution of Genotype–Phenotype Relationships. *Theoretical Population Biology* 57, 187-195.

Wilson, R.J. (2009). Introduction to graph theory, 4 edn (Edinburgh Gate, Harlow, Essex CM20 2JE, England: Prentice Hall).

Wotton, K.R., Jiménez-Guri, E., Crombach, A., Janssens, H., Alcaine-Colet, A., Lemke, S., Schmidt-Ott, U., and Jaeger, J. (2015). Quantitative system drift compensates for altered maternal inputs to the gap gene network of the scuttle fly *Megaselia abdita*. *eLife* 4, e04785.

Wray, G.A. (2007). The evolutionary significance of cis-regulatory mutations. *Nature Reviews Genetics* 8, 206-216.

Zheng, J., Payne, J.L., and Wagner, A. (2019). Cryptic genetic variation accelerates evolution by opening access to diverse adaptive peaks. *Science* 365, 347-353.